Synoptic Solar Physics
ASP Conference Series, Vol. 140, 1998
K. S. Balasubramaniam, J. W. Harvey and D. M. Rabin, eds.

Radio Synoptic Maps and Polar Cap Brightening

Kiyoto Shibasaki

Nobeyama Radio Observatory
Minamimaki, Minamisaku, Nagano 384-1305, Japan

Abstract. Radio synoptic maps at 17 GHz were synthesized from five years of daily full disk images by the Nobeyama Radio Heliograph (NRH). These synoptic maps were compared with soft X-ray and photospheric magnetic field synoptic maps. A radio butterfly diagram was also synthesized from the synoptic maps. One of the most prominent features of the radio synoptic maps is bright areas in the polar regions (polar cap brightening). Annual variation of the polar brightening area is clearly seen in the butterfly diagram. We found that the polar cap brightening is a limb brightening effect superposed on the bright features intrinsic to the polar regions. A gradual expansion of the polar brightening area towards low latitude was found in the north polar region during the declining phase of the solar activity cycle 22. It is proved that the Nobeyama Radio Heliograph is a suitable instrument for synoptic studies of the Sun.

1. Introduction

Long term measurements of radio emission from the Sun have a history of fifty years (Solar Activity Report, 1997). They are total flux measurement in the microwave range. It was shown that these data are good indices of solar activity (Schmahl & Kundu 1994). Spatially resolved routine observations of the Sun in the microwave region were initiated by Christiansen (1953) and Tanaka & Kakinuma (1992) using one-dimensional multi-element radio interferometers and extended to two dimensions. Large single dishes have been used for mapping the Sun. However, due to long wavelength of the microwave and the limited size of interferometers and that of dishes, spatial resolutions were not high enough to be comparable to routine optical observations. Short wavelength (millimeter or sub millimeter) observation by large single dish could overcome this limitation (e.g. Horne et al. 1980; Kosugi et al. 1986; Lindsey et al. 1990). Construction of large scale radio interferometers such as Westerbork Synthesis Radio Telescope and Very Large Array made it possible to have a similar spatial resolution with optical observation in the microwave region. However, solar observing time has been very limited with these large millimeter single dishes or large scale radio interferometers. Synoptic study of the radio Sun with high spatial resolution was not possible. This situation had changed by the construction of the Nobeyama Radio Heliograph (NRH) in 1992 (Nakajima et al. 1994). Daily radio images with high spatial resolution made it possible to synthesize synoptic maps comparable to optical synoptic maps.

There are several emission mechanisms working in the solar atmosphere at microwave range (Dulk 1985). Interpretation of radio data is sometimes difficult because of the multiple emission mechanisms. However, in the quiet Sun, most of the emission is free-free emission of the hot plasma in the upper chromosphere and above. In the active region, just above the large sunspot with strong magnetic field, gyroresonance emission causes very bright and compact emission. These two are the emission mechanisms working on the non-flaring Sun at 17 GHz.

In the following sections, radio synoptic map synthesis and features on the synoptic maps with emphasis on polar cap brightening are discussed.

2. Observation and Radio Emission Mechanism

2.1. Observation

Radio images of the Sun have been observed by the Nobeyama Radio Heliograph (NRH) since 1992. The NRH is a solar dedicated radio interferometer which can synthesize full disk solar images with 10 arcsecond spatial resolution at 17 GHz. Dual frequency observation at 17 and 34 GHz started on November 1995. In this paper, we use images only at 17 GHz. Observations are in routine mode and the time coverage of daily observation is from 23 UT to 07 UT. Temporal resolution is one second for usual mode. The key features of the NRH are listed in Table 1.

Table 1. Key Features of the Nobeyama Radio Heliograph

Field of View	:	Full Sun
Spatial Resolution	:	10(18) arc seconds
Temporal Resolution	:	1 second (50 msec for spiky events)
Frequency	:	17 GHz (+34 GHz, since Nov. 1995)
Polarization	:	RCP and LCP
Routine Observation	:	since July 1992
Daily Observation	:	23 UT $\sim$ 07 UT

Optical thicknesses of the terrestrial atmosphere and clouds at 17 GHz are not so large as at optical wavelengths. We can observe the Sun even in cloudy and rainy conditions. So the data coverage of the NRH is rather continuous. Heavy rain and wet snow pileup on the surface of parabolas cause severe absorption of radio signals from the Sun, when no images are available.

The NRH is a radio interferometer. The output signals from interferometers are spatial Fourier components (visibilities) of the brightness distribution on the sky corresponding to the baseline vectors normalized by the wavelength (e.g. Thompson et al. 1986). Inverse Fourier transformation of the observed visibilities results in the radio image, after phase and amplitude corrections. The shortest baseline vector of the antenna array determines the field of view, which covers the whole Sun in the NRH. The longest baseline vector determines

the highest available spatial resolution, which is 10 arcsecond with the NRH. The spatial resolution of the synthesized image depends also on the density of sampled Fourier components and also the weighting function in the visibility space. In the current study, we used all the available antenna pairs in equal weight. The resultant spatial resolution is about 18 arc seconds. This selection is for better image quality of extended weak features. RMS noise level of ten second integrated images are a few hundred Kelvin (Koshiishi 1996).

Differential phase fluctuations of the radio signals by turbulence of terrestrial atmosphere over the antenna arrays (about 500 m) cause deterioration of image quality. This radio seeing effect can be removed by use of the redundancy in the antenna array (Noordam & de Bruyn 1982). It is based on the principle that the output signal from pairs of antennas with the same baseline vectors should give the same phase if there are no phase errors. We can estimate phase errors of each antenna from the redundant output taken simultaneously with the visibility data for imaging and correct them. We can get stable radio images.

Image restoration is applied after the inverse Fourier transformation. Sampling coverage in the visibility space of the NRH is not full. There are many holes which cause high sidelobes. To suppress these sidelobes, we use the CLEAN method. There are several versions of the CLEAN method, among them we selected the one proposed by Steer et al. (1984) and it was implemented by Koshiishi (1996). This method can CLEAN extended features very quickly, and is best suited for the quiet Sun image restoration.

We use brightness temperature as a unit of radio brightness in case of resolved radio images. Radio flux, in a unit solid angle is converted to the temperature via the Rayleigh-Jeans' law of radiation. We normalize the median value of the quiet Sun disk as 10^4 K (Zirin et al. 1991) after image synthesis. This normalization makes it possible to get stable temperature scaling even during strong attenuation due to clouds or rain. We cannot recover long term variation of the quiet Sun value itself. This should be done by accurate total flux measurements.

2.2. Radio emission mechanism

Several emission mechanisms are working on the Sun at 17 GHz (e.g. Dulk 1985). Among them, f-f emission by thermal plasma in the upper chromosphere, transition region, and corona is the main emission mechanism of the quiet Sun. In this case, the observed brightness temperature is related to the physical temperature and the density of the solar atmosphere in the following way:

$$\begin{aligned} T_b &= \int T e^{-\tau} d\tau, \\ \tau &= \int \kappa d\ell, \\ \kappa &= \xi N^2/(f^2 T^{3/2}), \end{aligned}$$

where, τ and κ are optical depth and absorption coefficient respectively, and

T : temperature (K),
N : electron density (cm^{-3}),
ℓ : length along the line of sight (cm),
f : observing frequency (Hz),
ξ : constant(0.15 in corona and 0.08 in chromosphere).

Absolute calibration of the quiet Sun disk center by Zirin et al. (1991) showed that the brightness temperature at 18 GHz is 10,300 K. We put the median value of the quiet Sun disk as 10^4 at 17 GHz. This means that the optical depth becomes thick in the upper transition region.

In the case of the solar atmosphere, optically thin high temperature–plasma is situated above low–temperature plasma. This causes limb brightening because the length of the line of sight (hence the column emission measure) in the higher temperature atmosphere increases as the distance increases from the disk center.

In a case when an optically thick cloud ($\tau \gg 1$) is situated high in the atmosphere, the brightness temperature is equal to the physical temperature of the cloud ($T_b = T_c$). $H\alpha$ dark filaments are optically thick at 17 GHz with $10^{10.5}\mathrm{cm}^{-3}$ electron density (Hirayama 1985) and broader than sub arcsecond. If the electron temperature of the filaments is lower than the upper chromosphere, we will see a depression. We call these radio dark filaments. If these filaments are located on the solar limb (prominences), they are observed as enhancements (radio prominences) against the sky background.

Actual observed values are the result of the T_b value convolved with the synthesized beam, which is roughly 18 arc seconds size. The brightness temperature of filamentary structures smaller than the beam size will be diluted depending on the filling factor of the filaments or prominences.

3. Synthesis of Radio Synoptic Maps and a Butterfly Diagram

Daily radio images around local noon ($\sim$ 03 UT) have been synthesized since July 1992. Ten second integrated data are used for image synthesis. CLEAN restoration is applied down to 1,000 K deviation from the flat disk using Steer's algorithm (Koshiishi 1996). Resultant images are converted into FITS format.

Synoptic maps were synthesized using these daily FITS images. The radio brightness temperature distribution on the disk was converted into Carrington longitude and heliographic latitude coordinates, then the data in longitude coverage of 40 degrees centered at the L_o (the Carrington longitude of the disk center) are used for the synoptic map synthesis. Each point on the synoptic map is the result of the average of three days data. In case of data missing for three or more consecutive days, the synoptic map has a gap.

More than 60 rotation maps were synthesized from the rotation number 1858 (July 1992) to 1924 (July 1997). I could not synthesize the rotation maps between 1900 and 1902 because of long data gap, when the Radio Heliograph was upgrading to dual frequency operation. Short data gaps in some of the rotation are due to snow pile up or hardware troubles. The synoptic map of the rotation number 1868 (April-May 1993) is shown in Fig. 1(a).

A butterfly diagram was synthesized using the 61 rotation maps. In each rotation, a one–dimensional latitudinal distribution was obtained by selecting the highest brightness temperature value along the longitude in each latitude. The synthesized butterfly diagram is shown in Fig. 2.

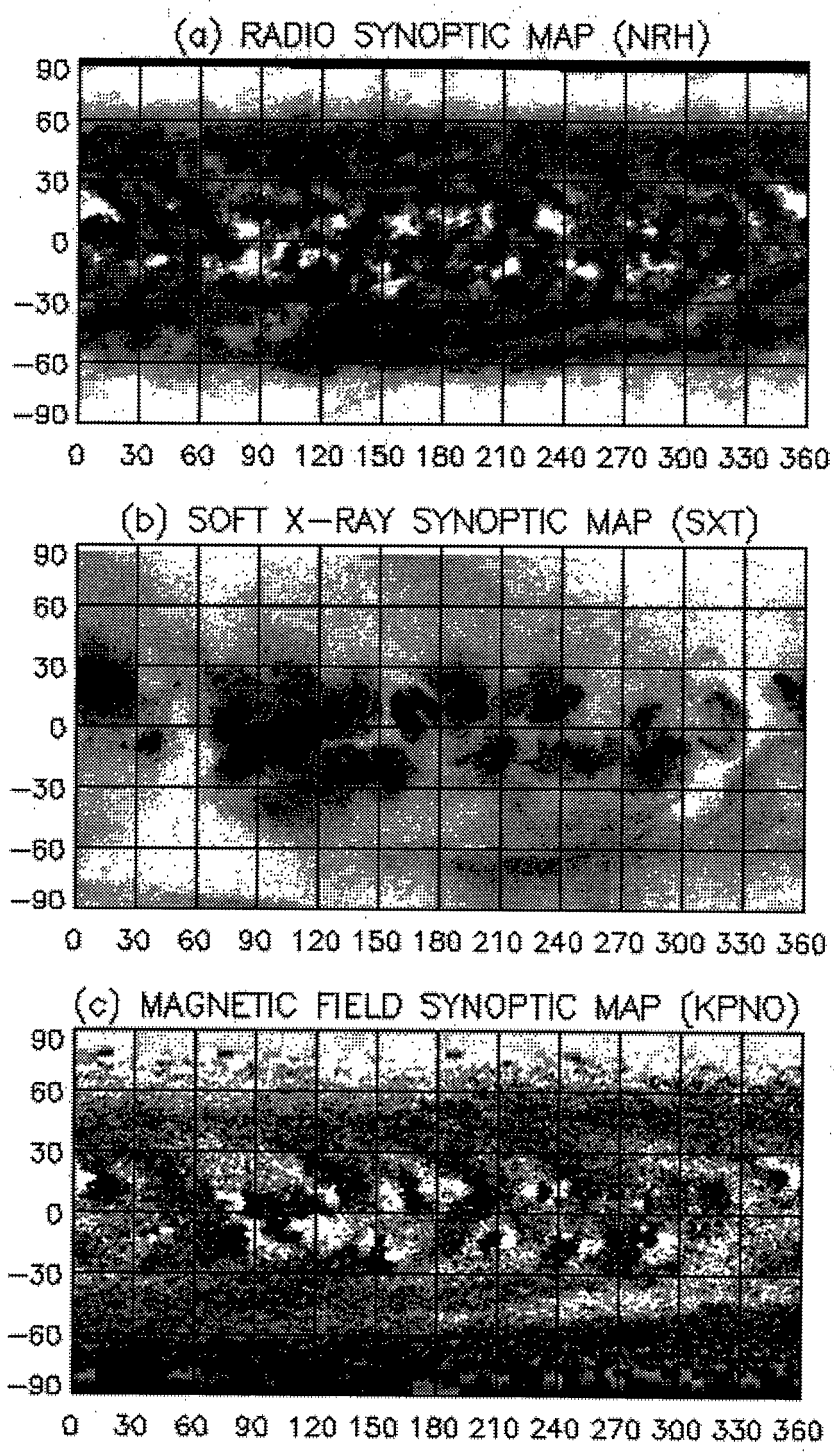

Figure 1. (a) Radio synoptic map of Carrington rotation 1868, $9,000K \leq T_b \leq 12,000K$, (b) Soft X-ray synoptic map of the same rotation in negative display, and (c) photospheric magnetic field synoptic map of the same rotation, $-20G \leq B_{||} \leq +20G$.

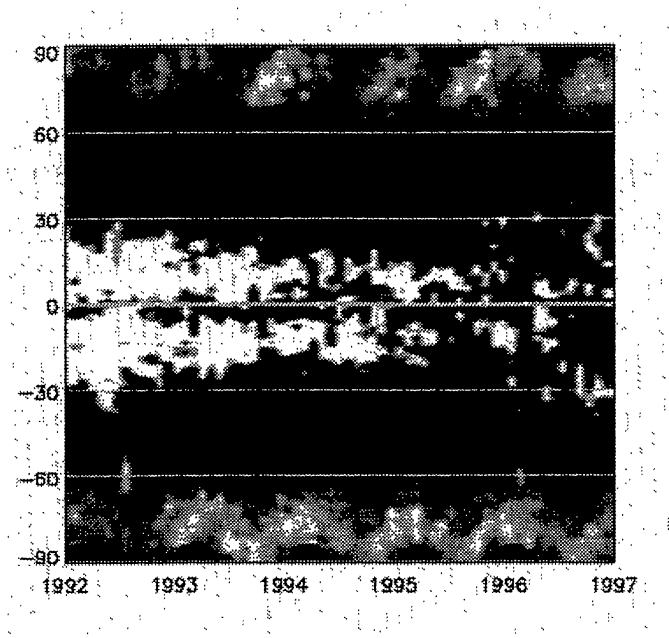

Figure 2. A radio butterfly diagram from July 1992 to July 1997

4. Comparison with Other Synoptic Maps

4.1. Synthesis of soft X-ray and magnetic field synoptic maps

Daily soft X-ray images observed by YOHKOH/SXT (Tsuneta et al. 1991) were used for the soft X-ray synoptic map synthesis. To cover large dynamic range of soft X-ray brightness, I used the composite images with short and long exposure time. The radius is fixed to that of the photosphere in the coordinate conversion. Positional shifts due to projection effects of high altitude sources are not taken into account in the synoptic map synthesis.

Daily longitudinal photospheric magnetic field distributions have been measured and synoptic magnetograms maps have been synthesized by the Kitt Peak National Observatory (NSO/KPNO). Projection effect of the magnetic field vector to the plane of the sky is corrected in the synoptic maps assuming that the fields are radial to the solar surface.

A set of synoptic maps (Carrington rotation 1868) of radio, photospheric magnetic field, and soft X-ray is shown in Fig. 1.

4.2. Radio dark features

Elongated dark features are collocated with polarity reversal lines of the photospheric magnetic field. These features are radio counterparts of $H\alpha$ dark filaments. Hence we call them radio dark filaments. $H\alpha$ dark filaments are optically thick at 17 GHz (Hirayama 1985). Observed brightness temperature depression is due to the lower temperature of the filaments than that of the upper transition region and diluted by the synthesized beam of the Radio Heliograph. Filling factor of the filamentary structure determines the darkness of the radio dark filaments. Radio brightness temperature depression was larger than 4,000 K for one of the radio dark filaments (N33, CL 265) on the synoptic map.

Much lower brightness temperature filaments down to 5,000 K can be found in daily images. Plasma temperature of these filaments need to be lower than or equal to 5,000 K. Radio dark filaments trace polarity reversal lines better or longer than $H\alpha$ filaments in quiet areas (Hiei et al. 1986).

Diffuse soft X-ray emission above the radio dark filaments, or shifted toward high latitude, suggest the closed coronal loops or arcades across the polarity reversal lines. One of the dark filament (S00 - S20 CL180) is associated with less bright X-ray features than the surrounding. It may correspond to a coronal cavity surrounding the dark filament (Tandberg-Hanssen 1974).

4.3. Radio bright features

There are several kind of bright features on the synoptic map. Brightest features are active regions. They are associated with strong soft X-ray emission and is located on the strong bipolar magnetic field region in general. Within some active regions, there exist very compact and bright (brighter than several tens of thousand Kelvin) radio sources just above a large sunspot, where soft X-ray emission is weak. The radio emission mechanism is not f-f but gyroresonance of thermal electrons gyrating around sunspot magnetic field (Shibasaki et al. 1994).

Next to active regions are polar cap brightening. During the minimum of activity, when there were no active regions on the disk, the brightest areas are polar regions. They are discussed in the next section.

There are diffuse and extended bright areas with several patchy features away from active regions, such as (1) N40 CL60 - N20 CL110, (2) S50 CL70 - S30 CL115, (3) S45 CL240 - S45 CL290, and (4) S40 CL300 - S20 CL320. Their excess brightness temperature from the quiet Sun level is 1,000 K or less. These features are associated with unipolar enhanced magnetic field regions. However, not all unipolar enhanced magnetic field regions are associated with radio enhancements. Two of the bright areas, (3) and (4), are located in a coronal hole. However, the coronal hole which extends from south polar region around CL55 does not accompany radio bright regions. The association of radio enhancements with unipolar enhanced magnetic field regions and with coronal holes was mentioned by Kosugi et al. (1986) and is still needs to be studied more extensively (Gopalswamy et al. in these proceedings).

Long lived X-ray bright points (such as at S05 CL308) are associated with radio bright points and also with small bipolar magnetic field regions. Their excess brightness temperature is 1,000 K or more.

5. Polar Brightening

5.1. Observational results

One of the most prominent features in the radio synoptic map at 17 GHz compared with other synoptic maps are bright features in polar regions. They consist of extended bright areas and patches around both polar regions. The excess brightness temperature reaches 4,000 K or more. Latitudinal profiles sampled every rotation (Fig. 3) show a gradual increase starting from 50 degrees.

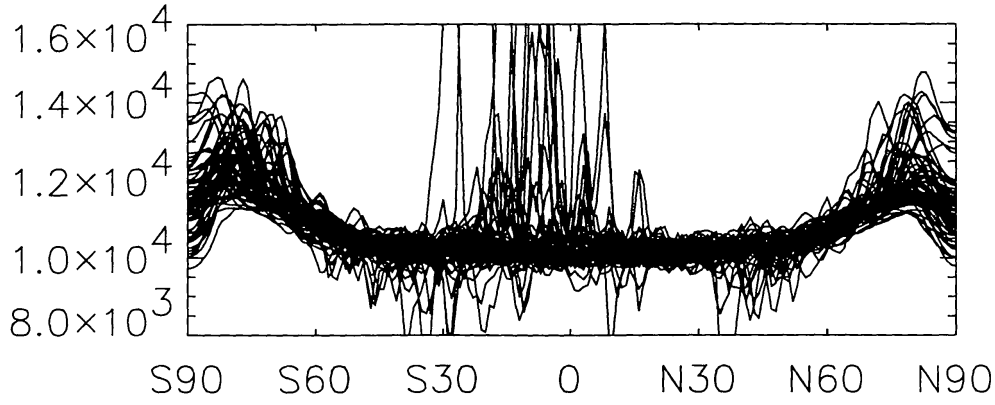

Figure 3. Superposition of north-south brightness profiles one per every rotation from July 1992 to July 1997.

Polar regions are often covered by coronal holes. Comparison of radio (Fig. 1(a)) and soft X-ray (Fig. 1(b)) synoptic maps show no one-to-one correspondence of polar coronal hole boundaries and radio enhancements.

In the synoptic magnetogram maps (Fig. 1(c)), we can see enhanced magnetic field regions in the southern high latitude region around S60 between CL240 and CL360. This region coincides with the extension of the polar cap brightening toward the lower latitude.

The butterfly diagram (Fig. 2) shows the sinusoidal variation of the polar cap brightening boundaries synchronized with the annual B_0 (heliographic latitude of the disk center) variation. This fact tells us that the polar cap brightening is a limb brightening.

To suppress the limb brightening effect, I synthesized a different kind of synoptic map. I picked up one dimensional north-south radio brightness profiles which cross the disk center every day. Five years of these profiles are aligned in Fig. 4. The abscissa is days and the ordinate is heliocentric latitude. Limb brightening variations are suppressed in this presentation. In this figure, we can still see the annual variation of the polar cap brightening boundaries which is anti phased with the variation in the butterfly diagram (Fig. 2). This variation tells us that the polar cap brightening is a phenomenon which is fixed to the polar region. These two components contribute to the polar cap brightening with similar amplitude.

As a result, the polar brightening is a limb brightening effect superposed on the bright features intrinsic to the polar regions.

5.2. Activity dependence

The butterfly diagram (Fig. 2) shows a gradual expansion of the bright area in the north polar region. The expansion rate is about one degree per year, about five degree expansion in five years. This period (1992 - 1997) corresponds to the declining phase of the 22nd activity cycle. So the expansion can be interpreted as an activity dependence. No activity dependence can be found in the south polar region. Fig. 4 shows that there is a bright region which extends from the

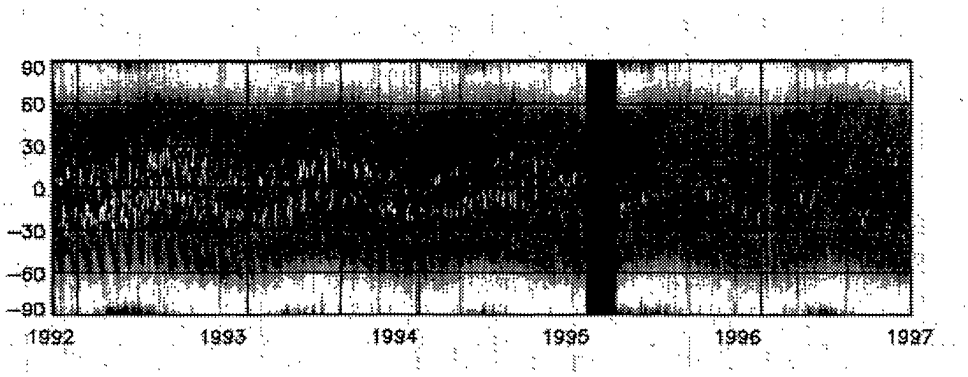

Figure 4. North-south brightness profiles from July 1992 to July 1997. Vertical lines are times when B_o is maximum.

south polar brightening region and is localized to a certain longitude range. This feature corresponds to the enhanced magnetic field region at the high latitude which is mentioned in the previous section (5.1). This feature may have obscured the activity dependence of the expansion of the bright area in the south polar region.

5.3. Interpretation

As mentioned in section 2.2, a stratified solar atmosphere will cause limb brightening. However, low latitude limbs do not show enhanced brightening. This can be interpreted by inhomogeneous solar atmosphere (e.g. Beckman et al 1973): low lying closed magnetic loops filled with low temperature and high density plasma suppress the limb brightening at short cm wavelength region. Enhanced limb brightening in polar region can be translated as non-effective suppression of limb brightening. Open or vertical field structure in the upper chromosphere in the polar regions will be the cause of the limb brightening. Polar plumes are good indicators of such field configurations in the polar regions.

So far, there is no evidence which can explain the extended intrinsic bright features of the polar regions. Polar regions are not bright in most of the spectrum except radio at short cm/mm. Detailed measurement of photospheric magnetic field in the polar regions may help to understand this component. Further study is required.

The lifetime of patchy structures is not long enough for a synoptic study. The time variability of the patchy structures in the polar regions and their association with other phenomena should be studied using high cadence image data such as SOHO/EIT simultaneously obtained with the radio images.

5.4. Discussion

Brightness enhancements in polar regions were first studied by Babin et al. (1976) and Efanov et al. (1980a,b) in short cm and mm wavelength regions using the Crimea 22-m dish. Higher spatial resolution observation by the Nobeyama 45-m telescope (Kosugi et al. 1986) with radial scanning method clearly showing the enhancement at 8.3 mm without any deconvolution processes. These observations are snapshot observations at certain phases of solar activity cy-

cles. Efanov et al. (1980a,b) pointed out that the polar bright areas appeared only during low activity period. With the NRH, we have been continuously monitoring the radio brightness distribution of the whole Sun with the spatial resolution of 18 arc second at the wavelength of 17.6 mm for more than five years, mainly the declining phase of the solar activity cycle 22. Koshiishi (1996) studied the polar cap brightening using the NRH data of 3 years of daily images processed by the Steer's algorithm which he implemented to the NRH image restoration. He used polar cap brightening boundary latitude and the area as the indices of the polar cap brightening. From the annual variation of these indices, he concluded that the polar cap brightening is different from a simple limb brightening and proposed a model that the polar cap brightening is the sum of the limb brightening and the brightening fixed to the pole region. Based on this model he showed that the north polar cap brightening region expanded gradually toward lower latitude in three years.

In the present study, we synthesized synoptic maps and butterfly diagram of the radio Sun for five years and reached the similar conclusion as that of Koshiishi (1996) more directly.

6. Summary and Conclusion

6.1. Nobeyama Radio Heliograph as a synoptic instrument

Most of the work done so far using data from the NRH concerns transient phenomena such as flares and prominence eruptions. In this study, it is proved that the NRH is also a suitable instrument for studies of synoptic solar physics.

Main features of the NRH which match synoptic observations are as follows: solar dedicated instrument, full Sun coverage, high spatial resolution (10 or 18 arc seconds), continuous observation (8hr/day, 5 years), little weather dependence, and seeing–free imaging.

Radio synoptic maps of Carrington rotation numbers 1858 - 1924 were synthesized and a butterfly diagram was synthesized from these rotation maps. A set of synoptic maps (rotation number 1868) of soft X-ray, photospheric magnetic field, and radio were compared.

Radio dark filaments are counterparts of $H\alpha$ dark filaments, and they trace polarity reversal lines better or longer than $H\alpha$ filaments in quiet area. The brightness temperatures of some of the dark filaments are as low as 5,000 K, where electron temperature of the filaments need to be lower than or equal to 5,000 K. Both filled in and empty cavity loops in the corona surrounding dark filaments are suggested from soft X-ray emission above them.

There are diffuse and extended radio bright areas away from active regions. Their excess brightness is 1,000 K or less. They are associated with unipolar enhanced magnetic field regions. Some of the low–latitude coronal holes have unipolar enhanced magnetic field region and are associated with radio enhancements.

6.2. Polar cap brightening

One of the most prominent features in the radio synoptic maps are polar cap brightenings. No other observations than short-cm/mm range show brightening

in polar regions. Their excess brightness is more than 4,000 K. Heliographic and heliocentric displays of the butterfly diagram show that the polar cap brightening is a limb brightening effect superposed on the bright features intrinsic to the polar regions. This conclusion is same as that of Koshiishi (1996). Two components contibute to the brightening with similar amplitude. Polar cap brightening is not directly related to polar coronal holes. Open field structures at the level of the upper chromosphere in the polar region will be the cause of enhanced limb brightening.

The northern polar cap brightening area showed expansion of one degree per year toward low latitude during the declining phase of the 22nd activity cycle.

Acknowledgments. The author wishes to thank the organizer of the workshop. The invitation by the organizers triggered this work. NSO/Kitt Peak data used here are produced cooperatively by NSF/NOAO, NASA/GSFC, and NOAA/SEL. YOHKOH is operated by ISAS, NASA and Yohkoh team members. The Nobeyama Radio Heliograph is operated by NAOJ/Nobeyama Solar Radio Observatory.

References

Babin A. N., Gopasyuk S. I., Efanov V. A., Kotov V. A., Moiseev I. G., & Tsap T. T. 1976, Izv. Krymsk. Astrofiz. Observ., 55, 3

Beckman J. E., Clark C. D., & Ross J. 1973, Solar Phys., 31, 319

Christiansen W. N. 1953, Nature, 171, 831

Dulk G. A. 1985, ARA&A, 23, 169

Efanov V. A., Labrum N., Moiseev I. G., Nesteorv N. S., & Steward R. T. 1980a, Izv. Krymsk, Astrofiz. Observ., 61, 52

Efanov V. A., Moiseev I. G., Nesterov N. S. & Stewart R. T. 1980b, in Kundu and Gergely (eds.), Radio Physics of the Sun, 141

Gopalswamy N., Shibasaki K., DeForest C. E., Bromage B. J. I., & Del Zanna G. 1998, these proceedings

Hiei E., Ishiguro M., Kosugi T. & Shibasaki K. 1986, in Poland A. I. (ed.) Coronal and Prominence Plasmas, NASA Conf. Pub. 2442, 109

Hirayama T. 1985, Solar Phys., 100, 415

Horne K., Hurford G., Zirin H., & de Graauw T. 1981, ApJ, 244, 340

Koshiishi H. 1996, Doctoral Thesis, University of Tokyo

Kosugi T., Ishiguro M. & Shibasaki K. 1986, PASJ, 38, 1

Lindsey C. A., Yee S., Roellig T. L., Hills R., Brock D., Duncan W., Watt G., Webster A., & Jefferies J. T. 1990, ApJ, 353, L53

Nakajima H., Nishio M., Enome S., Shibasaki K., Takano T., Hanaoka Y., Torii C., Sekiguchi H., Bushimata T., Kawashima S., Shinohara N., Irimajiri Y., Koshiishi H., Kosugi T., Shiomi Y., Sawa M., & Kai K. 1994, Proc. IEEE, 82, 705

Noordam J. & de Bruyn A. 1982, Nature, 299, 577

Schmahl E. & Kundu M. 1994, Solar Phys., 152, 167

Shibasaki K., Enome S., Nakajima H., Nishio M., Takano T., Hanaoka Y., Torii C., Sekiguchi H., Kawashima S., Bushimata T., Shinohara N., Koshiishi H., Shiomi Y., Irimajiri Y., Leka K. D., & Canfield R. 1994, PASJ, 46, L17

Solar Activity Report for April, 1997, Dominion Radio Astropysical Observatory

Steer D. G., Dewdney P. E., & Ito M. R. 1984, A&A, 137, 139

Tanaka H. & Kakinuma T. 1952, Rep. Res. Inst. Atmospherics, Nagoya U., 3, 55

Tandberg-Hanssen E. 1974, Solar Prominences, Geophysics and Astrophysics Monographs 12, D. Reidel Publishing Company, Dordrecht-Holland

Thompson A. R, Moran J. M. & Swenson G. W. 1986, "Interferometry and Synthesis in Radio Astronomy", A Wiley-Interscience , New York

Tsuneta S., Acton L., Bruner M., Lemen J., Brown W., Caravalho R., Catura R., Freeland S., Jurcevich B., Morrison M., Ogawara Y., Hirayama T., & Owens J. 1991, Solar Phys., 136, 37

Zirin H., Baumert B. M., & Hurford G. J. 1991, ApJ, 370, 779

Group Discussion

White: Very nice observations and presentation.

Shibasaki: Thank you.

Gopalswamy: It is known for a long time that the spicules are taller in the polar regions compared to the equatorial region. Also, the polar plumes populate the coronal holes. Can this difference account for the difference in limb brightening between the polar and equatorial regions?

Shibasaki: Taller spicules and polar plumes suggest radial structure of the atmosphere in the polar region. This will be the cause of enhanced (or little suppression of) limb brightening in the polar region.

Penn: Do you see any time variation of the polar brightenings on short (hour) timescales?

Shibasaki: Polar brightening consists of a broad enhancement which I discussed in my talk, and compact components which I did not discuss today. The compact components do show short timescale changes. We are now doing extensive study of the comparison of SOHO high cadence images of polar regions and Nobeyama Radio Heliograph images taken simultaneously.

Ruzmaikin: The polar cap brightenings seem to extend down to 60° latitude. Is there a reason for such a temperature variation?

Shibasaki: So far, no such evidence exists except microwave region. That is the reason why I am suggesting limb brightening explanation.

van Ballegooijen: The extension of the polar emission to latitudes of ±65 degrees is similar to that of polar magnetic fields measured at NSO/Kitt Peak. Why do you think that an addition to limb effect is required?

Shibasaki: The butterfly diagram of radio maps shows that the latitude of the extension of the polar brightening changes with B_o. This result denies that the polar brightening is fixed to a certain latitude range. There is a component which is fixed to a certain latitude range, as I showed in my talk. I want to compare the radio synoptic map with Kitt Peak magnetogram synoptic map, in which the projection effect in the polar region is corrected, to find the relation of this component to the enhanced magnetic field in the polar region.

Jones: Is the spatial scale of the inhomogeneous material which suppresses limb brightening in non-polar regions resolvable with your instrument?

Shibasaki: No, we cannot. We can detect the structures convolved with the beam size of 18 (10) arcseconds. Radio images do not show find structures of the beam size near disk center.